

# Easy and One-Step Synthesis of Ir Single Atom Doped PPy Nanoparticles for Highly Active N-Alkylation Reaction

Mariagrazia Iuliano,<sup>[a]</sup> Maria Sarno,<sup>\*[b, c]</sup> Claudia Cirillo,<sup>[a]</sup> Eleonora Ponticorvo,<sup>[a, c]</sup> and Salvatore De Pasquale<sup>[b, c]</sup>

Single atoms are nowadays considered new catalysts offering a lot of advantages such as reduced cost and use of noble metals. Here, we report the catalytic activity towards N-alkylation reactions of single atoms (SACs) of iridium doped polypyrrole (Ir-PPy nanoparticles). The new nanocatalyst exhibits excellent behavior due to the combination of highly active SACs catalyst and the organic conductive support providing strong binding of single atoms and thus improved reusability and easiness to

handle. In the presence of a low amount of Ir and of a suitable base, excellent activity (yield >99%) and selectivity (>99%) were obtained. In the optimized Ir condition (3 wt.% of Ir) an aniline conversion of about 99%, with excellent selectivity, just after 600 min, was obtained. Recyclability tests show that the catalyst can be successfully recycled six times without significant catalyst activity loss.

## Introduction

Thanks to huge applications in the synthesis of organic compounds, amines have been the object of a lot of studies.<sup>[1]</sup> Indeed, amines, especially aromatic, are intermediates for the production of pharmaceuticals, colorants, polymers, and agrochemicals.<sup>[1]</sup> N-alkylated amines can be prepared by a lot of methods.<sup>[2]</sup> These methods often suffer from environmental problems, the use of expensive starting materials, and low selectivity for the desired product. The N-alkylation of primary amines with alcohols, through "borrowing hydrogen", to produce secondary amines is an alternative and atom efficient approach.<sup>[3]</sup> This method has been documented as a "green" and concrete approach for the formation of carbon-carbon or carbon-nitrogen bonds. It does not involve pre-modification of the substrates or oxidants/reductants and provides water as the only by-product. In particular, it consists of: (i) alcohol dehydrogenation to give a carbonyl compound; (ii) reaction of the carbonyl group with an amine to reconstitute a condensation product; (iii) transfer of hydrogen atoms to the condensation product to form the final product. N-alkylation reactions have been studied in the presence of homogeneous transition metal

catalysts such as ruthenium (Ru), iridium (Ir), platinum (Pt), silver (Ag), and palladium (Pd) complexes.<sup>[4]</sup> However, these catalysts are characterized by some problems, such as the recovery of expensive metals and the use of metal complexes. The development of recoverable and effective catalysts to overtake these difficulties is now still challenging. Recently, heterogeneous inorganic-supported transition metal catalysts have been studied, such as Ru,<sup>[5a]</sup> Au,<sup>[5b]</sup> Pd.<sup>[6]</sup> On the other hand, typically, harsh conditions and/or poor selectivity was observed. Atomically dispersed catalysts on supports, as mononuclear metal complexes or single metal atoms, named as single-atom catalysts (SACs), are nowadays considered as new catalysts. They are characterized by full metal dispersion and utilization, SACs offer the best strategy for generating cheaper catalysts and utilization of noble metals.<sup>[7]</sup> Single-atom catalysts exhibit superior performance to be considered as the next-generation catalysts.<sup>[8]</sup> This is due to the lack of coordination, which allows easy anchoring to substrates, forming tough connections that favor charge-transfer processes. They don't suffer from particle size effects and they lack a surface, avoiding the adsorption step and allowing reaction in solution or gas phases. Although single atoms are a successful approach to minimize catalyst loading, a fine dispersion on supports avoiding aggregation is required. Intrinsic organic supports functionalities can provide stronger binding of single atoms and thus improved reusability and are easier to handle.<sup>[9a]</sup> In particular, polypyrrole (PPy) is increasingly studied<sup>[9]</sup> for many applications due to its good electrical conductivity, environmental and thermal stability, and ease of synthesis.<sup>[10]</sup> Conductive polymers,<sup>[11]</sup> such as PPy, are characterized by easy exchanges of electrons and are particularly useful where these exchanges take place. Here we report, for the first time, the catalytic activity towards N-alkylation reactions by using single atoms of iridium doped polypyrrole (Ir-PPy nanoparticles). These nanoparticles were obtained through a one-step microemulsion approach at room temperature. SACs of iridium can be dispersed and stabilized in the polypyrrole matrix. In particular, the N-alkylation of aniline with

[a] M. Iuliano, C. Cirillo, E. Ponticorvo  
Department of Industrial Engineering,  
University of Salerno  
Via Giovanni Paolo II, 132 – 84084 Fisciano (SA), Italy

[b] Prof. M. Sarno, Prof. S. De Pasquale  
Department of Physics "E.R. Caianiello"  
University of Salerno  
Via Giovanni Paolo II, 132 – 84084 Fisciano (SA), Italy

[c] Prof. M. Sarno, E. Ponticorvo, Prof. S. De Pasquale  
NANO\_MATES Research Centre  
University of Salerno  
Via Giovanni Paolo II, 132 – 84084 Fisciano (SA), Italy  
E-mail: msarno@unisa.it  
<http://docenti.unisa.it/maria.sarno>  
<https://www.nanomates.unisa.it>

Supporting information for this article is available on the WWW under <https://doi.org/10.1002/ejic.202000971>

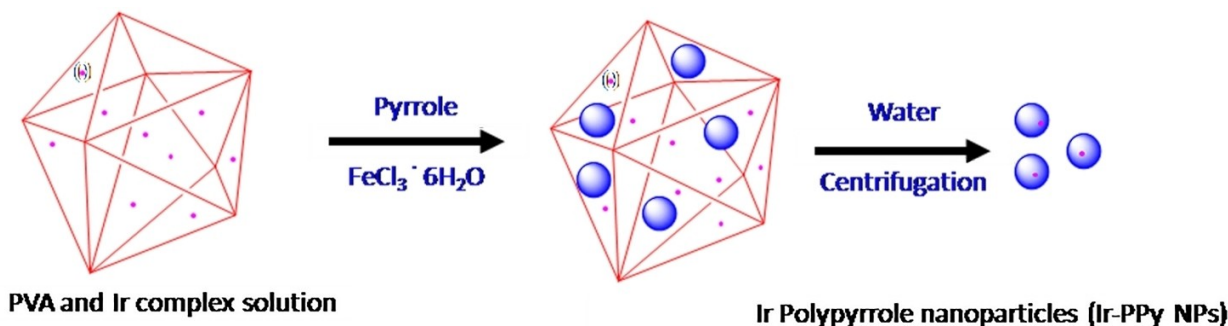


Figure 1. Schematic synthesis of Ir-PPy nanoparticles.

benzyl alcohol as an alkylating agent was investigated with different bases and different alkylating agents, showing high conversion and selectivity, in the presence of a low amount of iridium, which is in the form of single atoms, in short times and mild conditions.

## Results and Discussion

### Characterization of the Ir-PPy NPs

The schematic representation of the Ir-PPy synthesis is shown in Figure 1. Homogeneous Ir-PPy NPs were obtained through a polymerization performed in a one-step micro-emulsion and by using  $\text{Fe}^{3+}$  as the oxidizing agent. Polyvinyl alcohol (PVA) was introduced to improve nanoparticle water solubility and biocompatibility. Iridium complexes were wrapped in the PPy nanoparticles during their formation by  $\pi-\pi$  interactions or non-covalent interaction. By centrifugation, the removal of excess free PVA was performed, and Ir-PPy NPs were obtained. The wide-angle powder XRD pattern of Ir-PPy is shown in Figure 2. The four peaks at  $2\theta \sim 11.5^\circ$ ,  $22.8^\circ$ ,  $29.4^\circ$ , and  $41.4^\circ$ <sup>[12]</sup> are due to PPy chains scattering. In particular, the broad peak at about  $29^\circ$  is related to the scattering of the interplanar spacing of amorphous PPy.<sup>[12d]</sup> The amorphous nature of the hydrated precursor is also visible in Figure 2. The more resolved diffraction peaks can be attributed to PPy regular arrays producing short crystallinity. The spacing between the planes of benzene rings in the adjacent PPy chains determines the diffraction peak at  $2\theta = 19^\circ$ .<sup>[12d]</sup> The spectrum of Ir-PPy shows more resolved peaks and increased crystallinity for the support, probably induced by Ir. No peaks from Ir can be detected. Transmission electron microscopy (TEM) images of PPy and Ir-PPy NPs are shown in Figure 3. In particular, Figure 3a shows a TEM image of PPy nanoparticle that has a size in the range 60–80 nm. Figure 3b, Figure 3c, and Figure 3e show, at different magnifications, images of Ir-PPy NPs. The images exhibit quasi-spherical nanoparticles with a size slightly smaller than those of PPy nanoparticles alone (in the range 50–70 nm with a peak at 60 nm, see the histogram in Figure 3c). EDX spectrum in Figure 3d shows the peaks from Ir and Cu of the TEM grid. No peaks from Fe can be detected, likely due to the significant

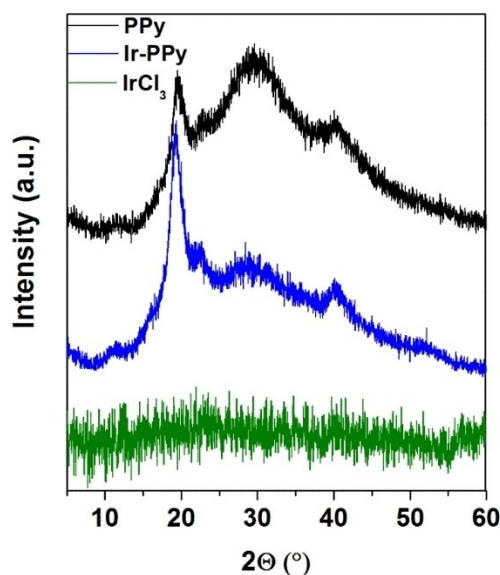
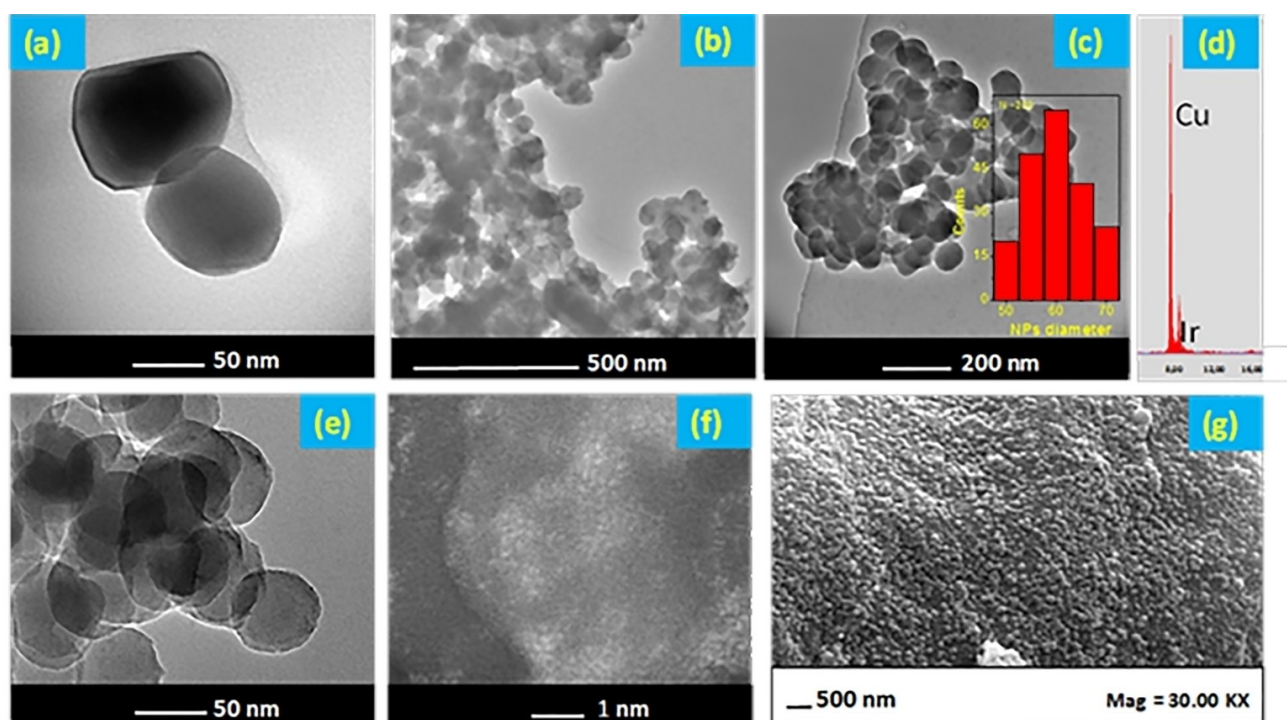


Figure 2. XRD spectra of PPy, Ir-PPy NPs and  $\text{IrCl}_3$  precursor.

difference between the redox potentials of iridium chloride and iron chloride, which decomposes much more easily. The Ir weight on the respect of PPy is equal to 1.95%, which is consistent with the amount of Ir loaded and indicating that Ir is preferentially localized on the surface of PPy NPs. Figure 3f shows the aberration-corrected HAADF/STEM image of the as-synthesized material.

In the image, contrast points coherent with single iridium atoms can be seen. Finally, Figure 3g illustrated the SEM image of Ir-PPy NPs, showing a spherical granular morphology for the sample consistent with that shown in the TEM image. The higher size exhibited by the nanoparticles can be ascribed to the gold coating used during the sample preparation for SEM. Ir, in the catalyst, was examined by CO-DRIFTS. CO symmetrical and asymmetrical stretching due to  $\text{Ir}(\text{CO})_2$  species, with mononuclear Ir, can be seen at  $2069\text{ cm}^{-1}$  and  $1989\text{ cm}^{-1}$ ,<sup>[13a]</sup> see Figure 4a.

The spectrum after 200 cycles of use is also reported in Figure 4a, showing the stability of the sample after usage. X-ray absorption fine extended structure (EXAFS) and X-ray absorp-



**Figure 3.** TEM images of: PPy NPs (a); Ir-PPy NPs (b, c, e). Ir-PPy EDX analysis (d). Aberration-corrected HAADF/STEM image of Ir-PPy (f). SEM image of Ir-PPy NPs (g).

tion energy near edge structure (XANES) spectroscopy, Figure 4b, were used to analyze the dispersion of Ir-SACs and their coordination environment. Ir/C was used as a benchmark. Ir single atom in Ir-PPy exhibits the main peak at ca. 1.5 c. On the other hand, Ir/C profile is dominated by a peak at about 2.35 c, which can be assigned to Ir-Ir scattering. It is worth noting that the Ir-Ir scattering is absent in the spectrum of Ir-SACs. The XANES spectra shown in Figure 4c, evidence a shift for Ir-SACs, green profile, indicating the Ir<sup>δ+</sup> form for Ir. In Figure 5, the thermogravimetric analysis profiles of PPy and Ir-PPy NPs are shown. It can be observed that the temperature range ~200 °C and ~300 °C is characterized by a sharp thermal degradation, accounting for a weight loss of up to 40%.

Ir-PPy NPs showed a slight up-shift of this first weight loss suggesting higher thermal stability for the Ir containing composite materials. FT-IR profiles of Ir-PPy NPs and PPy are shown in Figure 6. The FT-IR spectrum of polypyrrole alone shows vibrational bands at 1690 cm<sup>-1</sup> and 1540 cm<sup>-1</sup> corresponding to C-N and C-C stretching. The peak at 1455 cm<sup>-1</sup> can be assigned to pyrrole ring vibrations. The peak at about 1270 cm<sup>-1</sup> is due to the breathing vibrations of the pyrrole ring, the peak at 1190 cm<sup>-1</sup> to C-N vibrations, and the peaks at 1049 cm<sup>-1</sup> and 907 cm<sup>-1</sup> to C-H in and out plane vibrations.<sup>[13b,c]</sup> What can be seen in the Ir-PPy spectrum is the appearance of the band at 1562 cm<sup>-1</sup> due to C-C vibration and the downshift of the band at 1190 cm<sup>-1</sup> occurring for C-N bonds. This is due to the coordination of iridium with the polymer, indicating the formation of a strong interaction between PPy and Ir single atom in the composite material.

### Catalytic N-alkylation

N-alkylation of aniline with benzyl alcohol was, initially, chosen as a model reaction (Figure 7), to examine the catalytic activity of Ir-PPy NPs. The results of the tests carried out by using the catalyst in the presence of different bases, and with bases or PPy alone, are reported for comparison in Table 1 and Table 2, Figures 8 and 10 and Figures S1-S11. The data show that the kinetic of imine formation is faster than that of hydrogenation to the secondary amine.<sup>[13d]</sup> In particular, in Table 1 and Table 2 the results of the tests performed with benzyl alcohol (1 mmol), aniline (1 mmol), catalyst (25 mg at 2 wt.% Ir), base (2 mmol), toluene (5 mL), at 100 °C and under N<sub>2</sub> were shown after 12 and 24 hours, respectively. Compounds 1 and 2 together with a number of other molecules were formed, depending on the operating conditions, catalyst and base chosen. The results shown in entry 1 and entry 2 of Table 2, in comparison with entry 0 (Figure S1), highlights the role of the bases allowing reagents conversion. Moreover, poor selectivity vs. compound 2, compare Figure S1, Figure S2, and Figure S3, was observed. The comparison between the two bases evidence that KOTBu allows a higher selectivity vs. compound 2, although azobenzene and other by-products were produced in a higher amount. In all three cases, the formation of benzaldehyde is observed, indicating borrowing hydrogen occurring in the system; the quantities are higher in the presence of the two bases. The reduction of the benzyl alcohol amount during the experiments is probably due to the conversion into benzaldehyde, which is more volatile. In the case of entry 2, the formation of

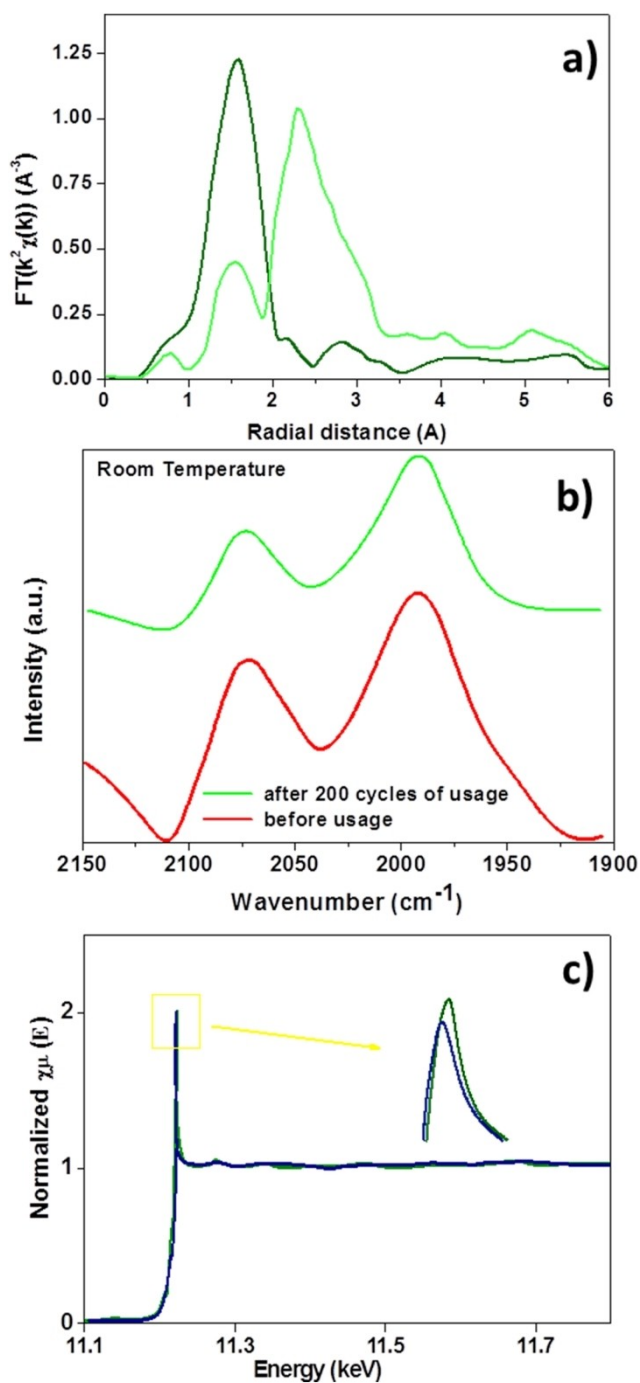


**Figure 4.** CO-DRIFT spectra of Ir-PPy before and after 200 cycles of usage (a). Fourier transforms of  $k^2$ -weighted Ir L3-edge EXAFS data for Ir-PPy and Ir/C (b). XANES of Ir L3-edge for Ir-PPy and Ir/C (c).

benzaldehyde appears more controlled over time, leading to the formation of component 1 with high selectivity. The presence of PPy, entry 3 and entry 4, Figure S4 and Figure S5, increases conversion and contributes to the formation of the amine. This suggests that PPy supports the base during the catalytic borrowing hydrogen process, likely with its ability to exchange electrons acting as a nucleophile and electrophile, as well. On the other hand, the selectivity towards the desired

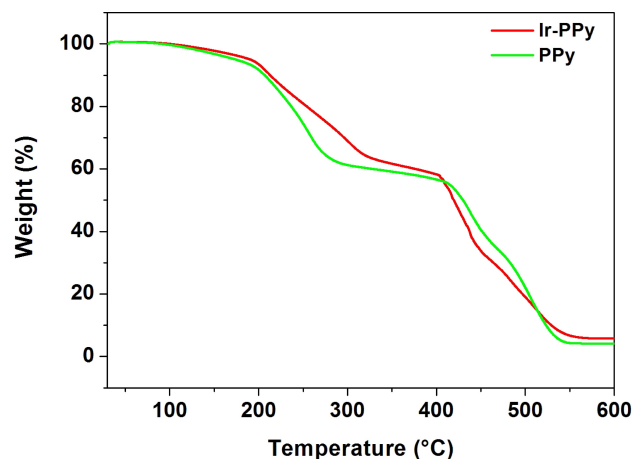


**Figure 5.** TGA profiles of PPy and Ir-PPy.

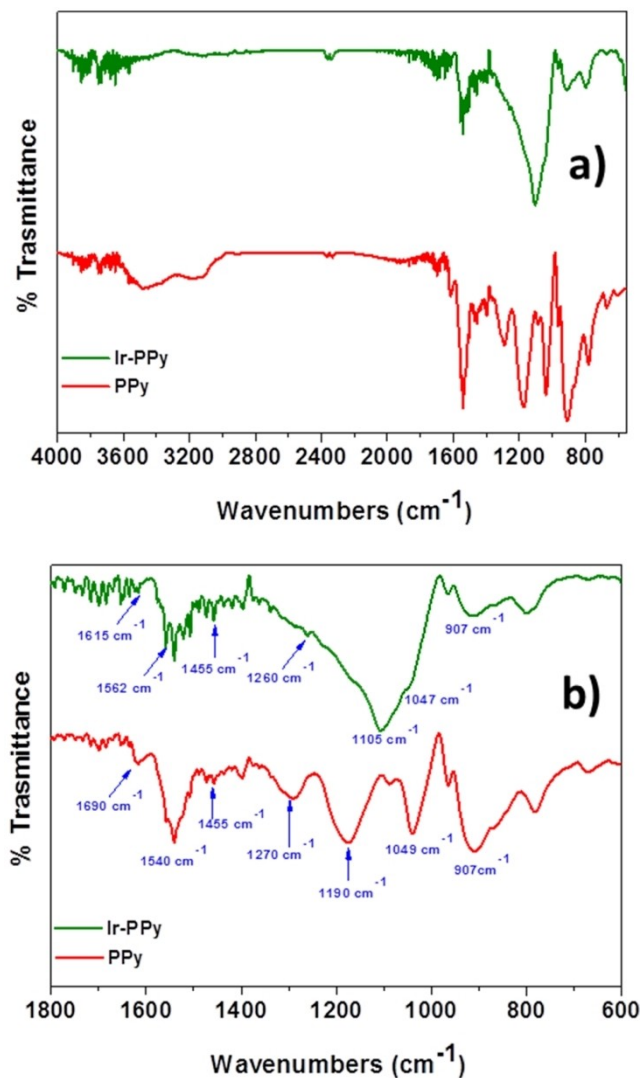


**Figure 6.** FT-IR spectra of PPy and Ir-PPy (a) and enlargement (b).

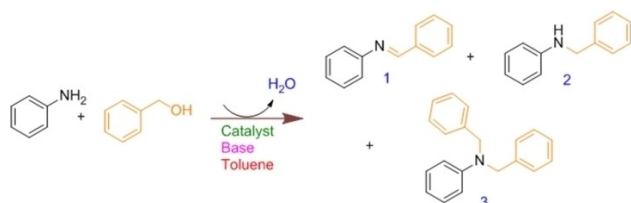


Figure 7. Schematic N-alkylation reactions of aniline with benzyl alcohol.

product is still low. In the case of entries 5 and 6, Figure 8 and Figure S6, the activity and selectivity towards products 1 and 2, due to the Ir presence, increase further; see the yield column in Table 2. The excellent behavior of the catalyst suggests that the formation of the imine is a surface limited step occurring on the active sites of Ir, where the reaction proceeds fastly. It is worth noticing that the differences in the selectivity vs. compound 2 obtained in the presence of the two bases are very large. Where KOTBu allows a very exciting result with a selectivity of 99%. In particular, in Figure 8a the evolution of conversion and selectivity to amine formation are reported during reaction time increase, in the case of KOTBu used as the base. Selectivity to secondary amine was higher than 75%, yet after 5 h. Moreover,

see Figure 8b, the formation of benzaldehyde supports the occurrence of hydrogen borrowing. It is to be underlined that the key role of the base in promoting catalysis is further evidenced by analyzing entry 7; see Figure S7, too. Low conversion, lower yield, and selectivity to compound 2 were observed. Other bases that, generally, give worse results have also been tested. In particular, the use of weaker bases, entry 8 and entry 9, show less activity. The potassium-containing base is able, in terms of selectivity, to provide better results, see Figure S8 and S9, also in this case. The yield further decreases by using even weaker bases, entry 10 (Figure S10). To better analyze the catalyst performance in the presence of KOTBu and aiming to reduce process times, further experiments were performed; see Figure 9 and Figure 10. As the content of Ir, Figure 9b, increases, the amount of benzyl alcohol available was reduced for each time, probably due to a faster formation of benzaldehyde, which is more volatile. Moreover, at 3 wt.% of Ir, the catalyst allows a quite total aniline conversion with excellent selectivity just after 600 min, see Figure 10.

The spectrum of Ir-PPy after 4 h of usage is dominated by new vibrational bands; see Figure 11. In particular, the bands at  $694\text{ cm}^{-1}$ ,  $762\text{ cm}^{-1}$ ,  $1316\text{ cm}^{-1}$ ,  $1377\text{ cm}^{-1}$ ,  $1452\text{ cm}^{-1}$ ,  $1587\text{ cm}^{-1}$ ,  $1591\text{ cm}^{-1}$  indicated the adsorption of benzylidene aniline. Additionally, the vibrational bands from benzylaniline

Table 1. N-alkylation of various amines with alcohol over Ir-PPy nanocatalyst.<sup>[a]</sup>

Entry	Catalyst	Base	Solvent	Conversion <sup>[b,f]</sup> [%]	Selectivity <sup>[b]</sup> [%]			Yield <sup>[b,f]</sup> [%] 2
					1	2	3	
0	PPy	-	Toluene	$5^{[e]} \pm 0.5$	$32 \pm 0.8$	$43 \pm 0.8$	-	< 3
1	-	KOTBu	Toluene	$30^{[c,e]} \pm 0.9$	$8 \pm 0.4$	$11 \pm 0.6$	-	< 8
2	-	NaOtBu	Toluene	$49^{[c]} \pm 0.4$	$98 \pm 0.4$	< 2	-	Trace
3	PPy	KOTBu	Toluene	$31^{[c,d,e]} \pm 0.5$	$5 \pm 0.2$	$44 \pm 0.4$	-	< 2
4	PPy	NaOtBu	Toluene	$55^{[c]} \pm 0.8$	$65 \pm 0.5$	$24 \pm 1.0$	-	$12 \pm 0.9$
5	Ir-PPy	KOTBu	Toluene	$75 \pm 0.8$	$6 \pm 0.7$	$94 \pm 0.4$	-	$70 \pm 0.5$
6	Ir-PPy	NaOtBu	Toluene	$59^{[c]} \pm 1.1$	$98 \pm 0.8$	$1 \pm 0.2$	-	Trace
7	Ir-PPy	-	Toluene	$10^{[c]} \pm 1.4$	$69 \pm 0.5$	$17 \pm 0.3$	-	< 3
8	Ir-PPy	KOH	Toluene	$65^{[c]} \pm 0.7$	$55 \pm 0.6$	$45 \pm 0.6$	-	< 29
9	Ir-PPy	NaOH	Toluene	$32^{[c]} \pm 0.7$	$74 \pm 0.1$	$25 \pm 0.7$	-	$8 \pm 0.5$
10	Ir-PPy	CsCO <sub>3</sub>	Toluene	$45 \pm 0.8$	$99 \pm 0.2$	< 1	-	Trace

[a] Reaction conditions: benzyl alcohol (1 mmol), aniline (1 mmol), catalyst (25 mg at 2 wt.% Ir), base (2 mmol), toluene (5 mL), 100 °C and under N<sub>2</sub>. [b] After 12 h. [c] Benzyl ether formation. [d] Bibenzyl formation. [e] Azobenzene formation. [f] Conversion and yield were determined by GC analysis using hexadecane as an internal standard.

Table 2. N-alkylation of various amines with alcohol over Ir-PPy nanocatalyst.<sup>[a]</sup>

Entry	Catalyst	Base	Solvent	Conversion <sup>[b,f]</sup> [%]	Selectivity <sup>[b]</sup> [%]			Yield <sup>[b,f]</sup> [%] 2
					1	2	3	
0	PPy	-	Toluene	$23^{[e]} \pm 0.7$	$23 \pm 0.5$	$47 \pm 0.4$	-	$10 \pm 0.7$
1	-	KOTBu	Toluene	$64^{[c,e]} \pm 2.1$	$10 \pm 2.2$	$12 \pm 1.0$	-	$10 \pm 1.6$
2	-	NaOtBu	Toluene	$50^{[c]} \pm 0.4$	$98 \pm 0.6$	< 1	-	Trace
3	PPy	KOTBu	Toluene	$97^{[c,d,e]} \pm 0.9$	< 1	$64 \pm 0.9$	-	$60 \pm 0.6$
4	PPy	NaOtBu	Toluene	$77^{[c]} \pm 0.6$	$60 \pm 1.0$	$21 \pm 1.1$	-	$16 \pm 0.8$
5	Ir-PPy	KOTBu	Toluene	> 99	< 0.7	> 99	-	> 99
6	Ir-PPy	NaOtBu	Toluene	$97^{[c]} \pm 0.4$	$97 \pm 0.3$	$1.5 \pm 0.2$	-	Trace
7	Ir-PPy	-	Toluene	$54^{[c]} \pm 1.5$	$77 \pm 0.5$	$18 \pm 1.3$	-	< 10
8	Ir-PPy	KOH	Toluene	$95^{[c]} \pm 0.9$	$24 \pm 1.2$	$72 \pm 0.9$	-	$68 \pm 0.3$
9	Ir-PPy	NaOH	Toluene	$97^{[c]} \pm 0.4$	$72 \pm 0.3$	$27 \pm 0.8$	-	$24 \pm 0.7$
10	Ir-PPy	CsCO <sub>3</sub>	Toluene	$94 \pm 0.7$	$94 \pm 0.4$	$6 \pm 0.5$	-	$5 \pm 0.9$

[a] Reaction conditions: benzyl alcohol (1 mmol), aniline (1 mmol), catalyst (25 mg at 2 wt.% Ir), base (2 mmol), toluene (5 mL), 100 °C and under N<sub>2</sub>. [b] After 24 h. [c] Benzyl ether formation. [d] Bibenzyl formation. [e] Azobenzene formation. [f] Conversion and yield were determined by GC analysis using hexadecane as an internal standard.

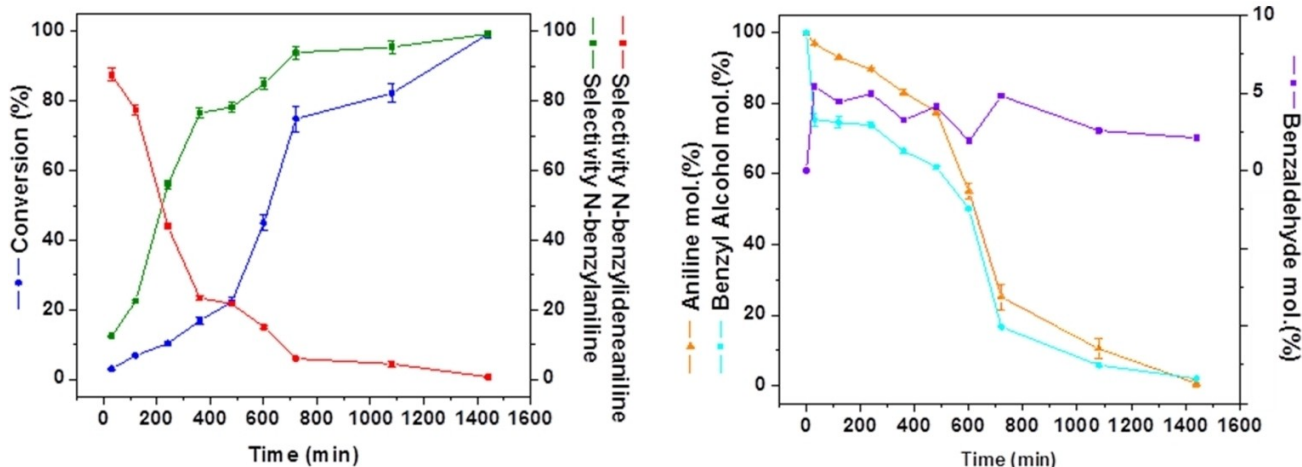


**Figure 8.** Effect of the time on conversion and selectivity of N-alkylation reaction in the presence of Ir-PPy NPs. Reaction conditions: benzyl alcohol (1 mmol), aniline (1 mmol), catalyst (25 mg 2 wt.% Ir), KOtBu (2 mmol), toluene (5 mL), 100 °C and under N<sub>2</sub>. Entry 5 Table 2.

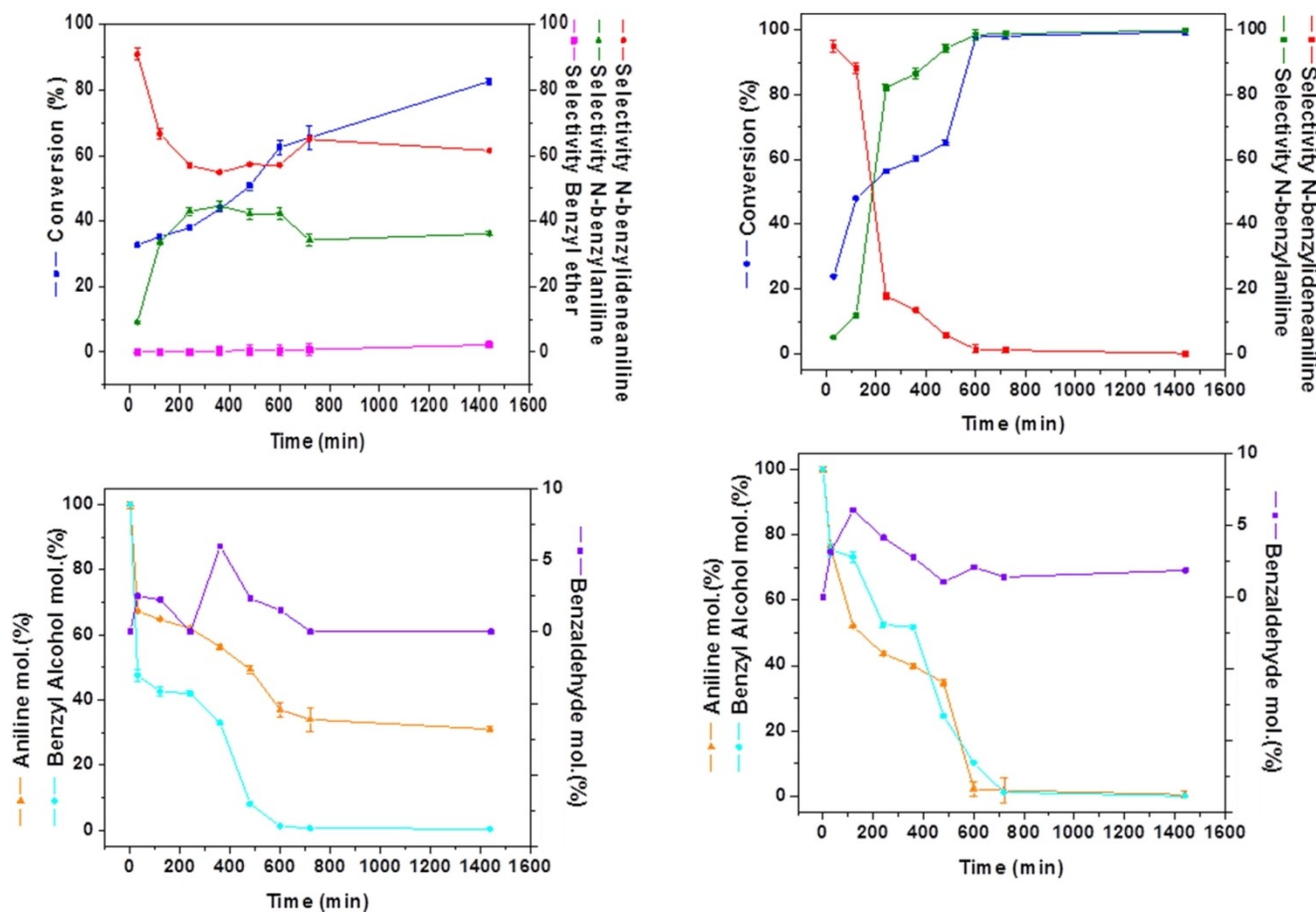


**Figure 9.** Effect of the time on conversion and selectivity of N-alkylation reaction in the presence of Ir-PPy NPs. Reaction conditions: benzyl alcohol (1 mmol), aniline (1 mmol), catalyst (25 mg 4 wt.% Ir), KOtBu (2 mmol), toluene (5 mL), 100 °C and under N<sub>2</sub>.

**Figure 10.** Effect of the time on conversion and selectivity of N-alkylation reaction in the presence of Ir-PPy NPs. Reaction conditions: benzyl alcohol (1 mmol), aniline (1 mmol), catalyst (25 mg 3 wt.% Ir), KOtBu (2 mmol), toluene (5 mL), 100 °C and under N<sub>2</sub>.

are also visible (values in green in the spectrum). More anchored benzaldehyde, probably to Ir sites, which vibrational

bands are hidden by higher benzylidene aniline presence before the thermal treatment up to 180 °C for 4 h in nitrogen flow, becomes visible at 1455 cm<sup>-1</sup> and 1591 cm<sup>-1</sup> after the

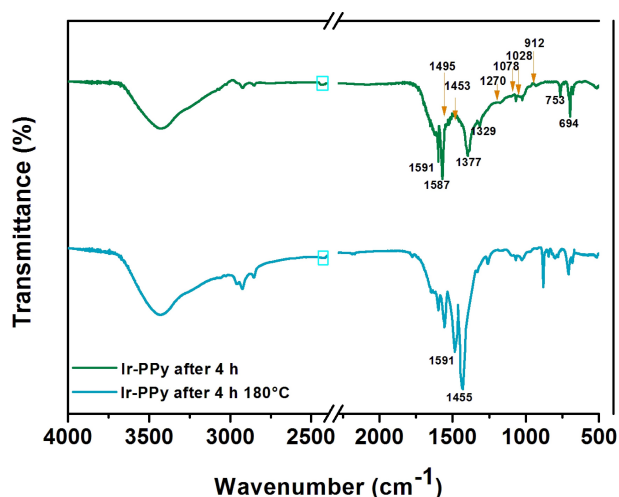


Figure 11. FT-IR spectra of Ir-PPy after 4 h of usage and after the treatment for 4 h at 180°C in nitrogen flow.

heating. Moreover, the FTIR spectrum in the range 2400  $\text{cm}^{-1}$ –2457  $\text{cm}^{-1}$ , see the light blue box in Figure 11, suggests the intermediate formation of Ir–H species.<sup>[13e]</sup>

On the base of the experimental observation, a mechanism for the N-alkylation on Ir-PPy was proposed in Figure 12, where the two different steps of imine formation and hydrogenation were shown. In particular, first of all, the bases are responsible for the alcohol deprotonation, since catalysis proceeds very slowly without the bases. The first step consists of forming an alkoxide on Ir active sites, followed by a condensation to form the imine on the same sites. Hydrogenation occurs more slowly, thanks to the hydride formed on the metal surface. Moreover, since it proceeds very differently with different bases and better with potassium based-bases, we have to consider a role for the base also in this process phase. The differences exhibited in the presence of NaOtBu and KOtBu can be ascribed to the higher electronegativity of K, which results in the ability to act as a bridge for hydrogen towards the formation of the secondary amine. Finally, it is not possible to exclude a role for the PPy surface, probably in supporting catalysis as an H<sub>2</sub> reservoir.

Other examples of N-alkylation of various amines with alcohols were reported in Table 3. The presence of N in the amine ring (2-amino pyridine) determines a reduction of

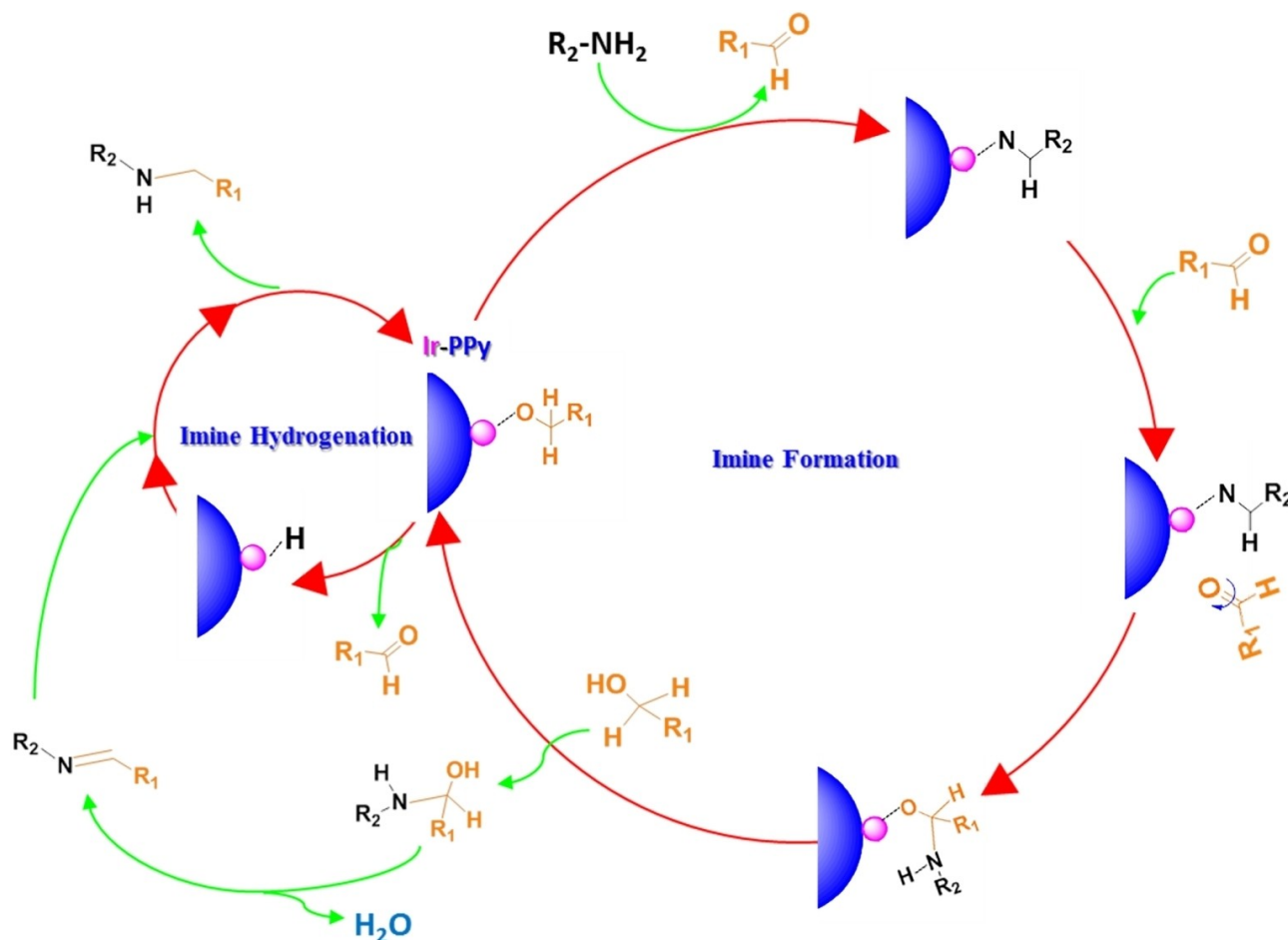


Figure 12. The proposed possible mechanism for Ir-PPy nanocatalyst for the N-alkylation reaction of aniline.

Entry	Amine	Alcohol	Targeted products	Conversion <sup>[b]</sup> [%]	Selectivity <sup>[c]</sup> [%]	Yield <sup>[b]</sup> [%]
1				> 99	> 99	> 99
2				> 98	> 98	> 99
3				97	96	94
4				96	95	91
5				94	92	80
6				93	94	88
7				> 99	> 99	> 99
8				98	> 99	98
9				> 99	> 99	98

[a] Reaction conditions: benzyl alcohol (1 mmol), aniline (1 mmol), catalyst (25 mg at 2 wt.% Ir), KOTBu (2 mmol), toluene (5 mL), 100 °C under N<sub>2</sub>, and 24 h of synthesis. [b] Conversion and yield were determined by GC analysis using hexadecane as an internal standard. [c] Selectivity of targeted products.

conversion, selectivity, and yield. Moreover, the substrate benzyl alcohol with electron-withdrawing Cl groups produced 80% and 88% yields of products.

### Recyclability of the nanocatalysts

We have studied the recyclability of the nanocatalyst; see Figure 13. The results highlight that the catalyst can be successfully recycled six times without any significant loss in catalytic activity. The slight decrease in product yield could be attributed to a small loss of the catalyst during the recycling process and probably to a feeble activity reduction due to the use.

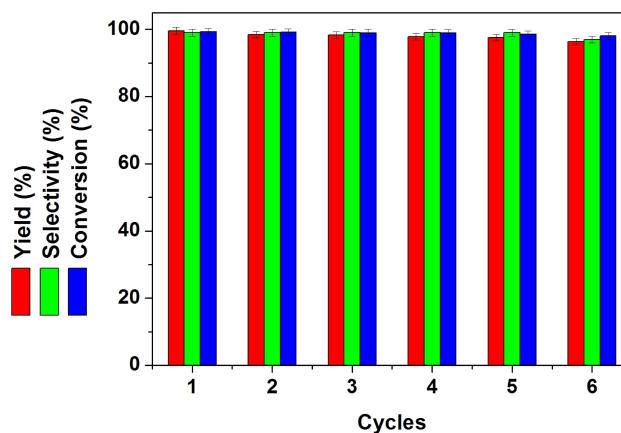


**Figure 13.** Recycling efficiency of Ir-PPy NPs in the N-alkylation of aniline. Reaction conditions: benzyl alcohol (1 mmol), aniline (1 mmol), catalyst (25 mg 2 wt.% Ir), KOTBu (2 mmol), toluene (5 mL), 100 °C and under N<sub>2</sub>.

## Conclusion

Morphological and structural characterization shows the formation of PPy nanoparticles covered by iridium single atoms anchored with the support. N-alkylation reactions with aniline and benzyl alcohol were examined in the presence of different bases and with and without PPy and Ir-PPy. The data show that the kinetic of imine is faster than that of hydrogenation to the secondary amine. The formation of benzaldehyde is observed, indicating that borrowing hydrogen occurs in the system. Activity, and selectivity towards products 1 and 2 increase, in the presence of Ir. The excellent behavior of the catalyst suggests that the formation of the imine is a surface limited step occurring on the active sites of Ir. KOTBu, in comparison with NaOTBu allows higher selectivity vs. compound 2. This is likely due to the higher electronegativity of K acting as a bridge for hydrogen towards secondary amine formation. Moreover, at 3 wt.% of Ir, the catalyst allows a very high aniline conversion, with excellent selectivity, just after 600 min, likely due to a large amount of Ir active sites, probably favoring benzaldehyde anchoring and evolution vs. the products. Recyclability tests show the catalyst stability without any significant loss in catalyst activity.

## Experimental Section

### Materials

Pyrrrole, iridium(III) chloride hydrate (IrCl<sub>3</sub>), iron(III) chloride hexahydrate (FeCl<sub>3</sub>·6H<sub>2</sub>O), polyvinyl alcohol (PVA), ethanol, distilled water, aniline, benzyl alcohol, toluene, potassium hydroxide (KOH), sodium hydroxide (NaOH), cesium carbonate (CsCO<sub>3</sub>), sodium tert-butoxide (NaOTBu), potassium tert-butoxide (KOTBu), dodecane (internal standard) and all other reagents and substrates were purchased from Sigma Aldrich.

### Synthesis of Ir-PPy nanoparticles

First of all, PVA (500 mg) and FeCl<sub>3</sub>·6H<sub>2</sub>O (500 mg) were mixed in deionized water (10 mL). Then, IrCl<sub>3</sub> was dissolved in 2 ml of ethanol under stirring for 30 min and added to the previously prepared solution. After that, pyrrole (70 μL) was added to the reaction mixture and stirred for 24 h. Iridium precursor was added to give an Ir loading of 2 wt.% pyrrole weight-based. After polymerization, the solution was washed and centrifuged. During the synthesis, lone pairs electrons in nitrogen atoms (existing in pyrrole monomer) can reduce Ir precursor. In this process, the role of PVA cannot be neglected, too. The Ir NPs generated and attached on the PPy matrix via π-π, or non-covalent interaction among N in PPy matrix and Pd occurs. PPy nanoparticles were also prepared with the same procedure but the absence of Ir precursor.

Ir/C consisting of Ir atoms and Ir nanoparticles dispersed on carbon was obtained through pyrolysis of and Ir precursor, too. In particular, Ir(acac)<sub>3</sub> was mixed under ultrasounds with Vulcan XC-72. After drying in vacuum conditions, the mixture was pyrolyzed under Ar/H<sub>2</sub> atmosphere (15 vol.% H<sub>2</sub>) at 320 °C for 3 h.

### Characterization techniques of Ir-PPy NPs

For Ir-PPy characterization: TEM (Transmission electron microscopy) (FEI-Tecnai; 200 KV) equipped with an Energy Dispersive X-ray Analysis (EDX) probe; High-resolution analytical TEM (F20 FEI Tecnai-200 kV) for high-angle annular dark-field (HAADF) analysis, with HAADF detector employed in STEM mode; SEM (Scanning electron microscope) (FESEM LEO1525), UV-Visible spectroscopic analysis (EVOLUTION S60, Thermo Fischer Scientific), XRD measurements (Bruker D8 X-ray diffractometer using CuKα radiation), thermogravimetric analysis (TG-DTG, SDTQ 600 Analyzer TA Instruments) at 10 K/min heating rate in airflow and FT-IR analysis (Vertex 70 apparatus (Bruker Corporation)), were performed. Thermo-Scientific Nicolet (i550 FTIR) was used for Diffuse Reflectance Infrared Fourier Transform spectroscopy (DRIFTS) measurements. CO flux, 25 mL/min, was provided for the reaction chamber, which was successively purged by a N<sub>2</sub> flow. XANES and EXAFS were obtained at beamline of the Elettra Synchrotron (x-ray beam 16–20 eV). The measurements were performed at room temperature. For the measurement a homogenous layer of the sample was prepared. Typically, 5 different scans were performed to reduce the signal-to-noise ratio. Data analysis was performed in agreement with ATHENA program pack.

### General procedure for the N-alkylation reactions over Ir-PPy

The N-alkylation reactions were carried out in a round-bottomed flask (capacity, 50 mL) at 100 °C under N<sub>2</sub> atmosphere. In a typical experiment, in 5 ml of toluene, aniline (1 mmol), benzyl alcohol (1 mmol), base (2 mmol), and Ir-PPy nanoparticles (25 mg) were added and heated up to 100 °C for a specific time. The progress of the reaction was monitored at different time intervals and quantified by gas chromatography-mass spectrometry (GC-MS, Thermo Fischer Scientific) analysis. After the reaction time, using a simple filtration, the nanocatalyst was removed. The mixture was dried over Na<sub>2</sub>SO<sub>4</sub>, and the residue was purified by flash column chromatography on silica gel. GC-MS was used for identified desired products. The Ir-PPy after filtration was washed with water several times and dried at 60 °C for further use.

### Product analysis

The products obtained by the N-alkylation of amines with alcohols were analyzed through a GC-MS (Thermo Fischer Scientific) equipped with a TG-POLAR capillary column (0.25 μm×0.25 mm×60 m). All reaction products were identified by matching the GC retention time with authentic samples. The column temperature was kept at 160 °C for 1 min, then raised to 270 °C at 3 °C/min and maintained at this temperature for 10 min. The temperatures of the injector and detector were set at 250 °C. Helium with a flow of 1.2 ml/min was used as the carrier gas. The qualitative analysis was compared with the chromatographic standard and mass spectrometry of the product. The obtained results were in good agreement with parallel evaluation performed by using hexadecane as an internal standard. The experiments were performed in triplicate. The texts, along with the results, are expressed with a standard deviation, to take into account the different results. The conversion of amine was calculated as follows:<sup>[14a]</sup>

$$(\%) \text{ of amine} = \frac{\text{Initial wt. \% of amine} - \text{final wt. \% of amine}}{\text{Initial wt. \% of amine}} * 100 \quad (1)$$

The product selectivity was calculated as:<sup>[14b]</sup>

$$\text{Selectivity } (\%) = \frac{\text{Peak area of product}}{\text{Total Peak area for all the products}} * 100 \quad (2)$$

The aniline mol % was calculated as

$$\text{Aniline mol. (\%)} = \frac{\text{mol of aniline}_t}{\text{initial mol of aniline}} * 100 \quad (3)$$

The Benzyl alcohol mol % was calculated as

$$\text{Benzyl alcohol mol. (\%)} = \frac{\text{mol of benzyl alcohol}_t}{\text{initial mol of benzyl alcohol}} * 100 \quad (4)$$

The Benzaldehyde mol % was calculated as

$$\text{Benzaldehyde mol \%} = \frac{\text{mol of benzaldehyde}_t}{\text{initial mol of benzyl alcohol}} * 100 \quad (5)$$

FT-IR spectra of the samples were obtained by using Vertex 70 apparatus (Bruker Corporation). Spectra were recorded in the scanning range from 4000 to 400 cm<sup>-1</sup>. <sup>1</sup>H NMR analysis was performed using Bruker Advance 400 (Operating at 400 MHz).

## Conflict of Interest

The authors declare no conflict of interest.

**Keywords:** Borrowing hydrogen · N-alkylation · Nanocatalysis · Nanoparticles · Reaction mechanisms

- [1] a) R. Dobler, I. Bruce, F. Cederbaum, N. G. Cooke, L. J. Diorazio, R. G. Hall, E. Irving, *Tetrahedron Lett.* **2001**, *42*, 8281–8284; b) S. A. Lawrence, *Amines: Synthesis, Properties and Application*, Cambridge University, Cambridge, **2004**.
- [2] a) T. O. Vieira, H. Alper, *Chem. Commun.* **2007**, 2710–2711; b) X. Shen, S. L. Buchwald, *Angew. Chem. Int. Ed.* **2010**, *49*, 564–567; c) X. Li, E. A. Mintz, X. R. Bu, O. Zehnder, C. Bosshard, P. Gunter, *Tetrahedron* **2000**, *56*, 5785–5791; d) T. Mizuta, S. Sakagushi, Y. Ishii, *J. Org. Chem.* **2005**, *70*, 2195–2199; e) O. Navarro, N. Marion, J. Mei, S. P. Nolan, *Chem. Eur. J.* **2006**, *12*, 5142–5148.
- [3] a) T. D. Nixon, M. K. Whittlesey, J. M. J. Williams, *Dalton Trans.* **2009**, 753–762; b) M. H. S. A. Hamid, P. A. Slatford, J. M. J. Williams, *Adv. Synth. Catal.* **2007**, *349*, 1555–1575; c) G. Guillena, D. J. Ramón, M. Yus, *Chem. Rev.* **2010**, *110*, 1611–1641; d) F. Alonso, P. Riente, M. Yus, *Acc. Chem. Res.* **2011**, *44*, 379–391; e) R. Yamaguchi, K.-I. Fujita, M. Zhu, *Heterocycles* **2010**, *81*, 1093–1140; f) Y. Obora, *ACS Catal.* **2014**, *4*, 3972–3981; g) C. Gunanathan, D. Milstein, *Science* **2013**, *341*, 1229712; h) L. Suntrup, S. Hohloch, B. Sarkar, *Chem. Eur. J.* **2016**, *22*, 18009–18018; i) V. Sankar, M. Kathiresan, B. Sivakumar, S. Mannathan, *Adv. Synth. Catal.* **2020**, *362*, 4409–4414; j) F. Niu, Q. Wang, Z. Yan, B. T. Kusema, A. Y. Khodakov, V. V. Ordonsky, *ACS Catal.* **2020**, *10*, 3404–3414.
- [4] a) A. B. Enyong, B. Moasser, *J. Org. Chem.* **2014**, *79*, 7553–7563; b) T. Ohshima, Y. Miyamoto, J. Ipposhi, Y. Nakahara, M. Utsunomiya, K. Mashima, *J. Am. Chem. Soc.* **2009**, *131*, 14317–14328; c) R. Kawahara, K.-I. Fujita, R. Yamaguchi, *Adv. Synth. Catal.* **2011**, *353*, 1161–1168; d) S. Ruch, T. Irgang, R. Kempe, *Chem. Eur. J.* **2014**, *20*, 13279–13285; e) C. Crotti, E. Farnetti, S. Licen, P. Barbieri, G. Pitacco, *J. Mol. Catal. A* **2014**, *382*, 64–70; f) B. Sreedhar, P. Surendra Reddy, M. Amarnath Reddy, B. Neelima, R. Arundhathi, *Tetrahedron Lett.* **2007**, *48*, 8174–8177; g) A. Martínez-Asencio, M. Yus, D. J. Ramón, *Synthesis* **2011**, *2011*, 3730–3740; h) T. T. Dang, B. Ramalingam, S. P. Shan, A. M. Seayad, *ACS Catal.* **2013**, *3*, 2536–2540.
- [5] a) J. W. Kim, K. Yamaguchi, N. Mizuno, *J. Catal.* **2009**, *263*, 205–208; b) T. Ishida, N. Kawakita, T. Akita, M. Haruta, *Gold Bull.* **2009**, *42*, 267–274.
- [6] a) M. H. S. A. Hamid, C. L. Allen, A. C. Maxwell, H. C. Maytum, A. J. A. Watson, J. M. J. Williams, *J. Am. Chem. Soc.* **2009**, *131*, 1766–1774; b) Y. Zhang, X. Qi, X. Cui, F. Shi, Y. Deng, *Tetrahedron Lett.* **2011**, *52*, 1334–1338.
- [7] a) M. Yang, L. F. Allard, M. Flytzani-Stephanopoulos, *J. Am. Chem. Soc.* **2013**, *135*, 3768–3771; b) P. X. Liu, Y. Zhao, R. X. Qin, S. G. Mo, G. X. Chen, L. Gu, D. M. Chevrier, P. Zhang, Q. Guo, D. D. Zang, B. H. Wu, G. Fu, N. F. Zheng, *Science* **2016**, *352*, 797–801.
- [8] a) J. Lin, A. Q. Wang, B. T. Qiao, X. Y. Liu, X. F. Yang, X. D. Wang, J. X. Liang, J. X. Li, J. Y. Liu, T. Zhang, *J. Am. Chem. Soc.* **2013**, *135*, 15314–15317; b) X. Guo, G. Fang, G. Li, H. Ma, H. Fan, L. Yu, C. Ma, X. Wu, D. Deng, M. Wei, *Science* **2014**, *344*, 616–619; c) G. Kyriakou, M. B. Boucher, A. D. Jewell, E. A. Lewis, T. J. Lawton, A. E. Baber, H. L. Tierney, M. Flytzani-Stephanopoulos, E. C. H. Sykes, *Science* **2012**, *335*, 1209–1212; d) H. Wei, X. Liu, A. Wang, L. Zhang, B. Qiao, X. Yang, Y. Huang, S. Miao, J. Liu, T. Zhang, *Nat. Commun.* **2014**, *5*, 5634.
- [9] a) D. Chandra, B. K. Jena, C. R. Raj, A. Bhaumik, *Chem. Mater.* **2007**, *19*, 6290–6296; b) K. Guerchouche, E. Herth, L. E. Calvet, N. Roland, C. Loyez, *Microelectron. Eng.* **2017**, *182*, 46–52; c) R. Jain, N. Jadon, A. Pawaiya, *TrAC Trends Anal. Chem.* **2017**, *97*, 363–373; d) I. Sapurina, Y. Li, E. Alekseeva, P. Bober, M. Trchova, Z. Moravkova, J. Stejskal, *Polymer* **2017**, *113*, 247–258; e) B. Yue, C. Wang, X. Ding, G. G. Wallace, *Electrochim. Acta* **2013**, *113*, 17–22; f) N. K. Guimard, N. Gomez, C. E. Schmidt, *Prog. Polym. Sci.* **2007**, *32*, 876–921.
- [10] a) G. Wallace, G. M. Spinks, L. A. P. Kane-Maguireand, P. Teasdale, *Conductive Electroactive Polymers*, CRC Press, New York, USA, **2003**; b) J. Y. Lee, S. H. Cho, K. T. Song, *Handbook of Conductive Polymers*, T. A. Skotheim, J. R. Reynolds, Eds., CRC Press, New York, USA, **2007**; c) S. Elangovan, J. Neumann, J.-B. Sortais, K. Junge, C. Darcel, M. Beller, *Nat. Commun.* **2016**, *7*, 12641.
- [11] a) A. Bayat, M. Shakourian-Fard, P. Nouri, M. M. Hashemi, *Appl. Organomet. Chem.* **2017**, *31*, e3720; b) A. Chen, H. Wang, R. Liu, Y. Bo, J. Hu, *Catal. Lett.* **2016**, *146*, 1182–1193.
- [12] a) E. A. Sanches, S. F. Alves, J. C. Soares, A. M. da Silva, C. G. da Silva, S. M. de Souza, H. O. da Frota, *J. Nanomater.* **2015**, *2015*, 1–8; b) W. Feng, E. Sun, A. Fujii, H. Wu, K. Niihara, K. Yoshino, *Chem. Soc. Jpn.* **2000**, *73*, 2627–2633; c) A. Dumitru, S. Vulpe, A. Radu, S. Antohe, *Rom. J. Phys.* **2018**, *63*, 605–625; d) Z. D. Kojabad, S. A. Shojaosadati, *Mater. Des.* **2016**, *96*, 378–384.
- [13] a) Y. B. Lu, J. M. Wang, L. Yu, L. Kovarik, X. W. Zhang, A. S. Hoffman, A. Gallo, S. R. Bare, D. Sokaras, T. Kroll, V. Dagle, H. L. Xin, A. M. Karim, *Nat. Can.* **2019**, *2*, 149–156; b) Xia, A. G. MacDiarmid, A. J. Epstein, *Macromolecules* **1994**, *27*, 7212–7214; c) M. A. Chougule, S. W. Sen, V. B. Patil, *Synth. Met.* **2012**, *162*, 1598–1603; d) M. V. Jiménez, J. Fernández-Tornos, M. González-Lainez, B. Sánchez-Page, F. J. Modrego, L. A. Oro, J. J. Pérez-Torrente, *Catal. Sci. Technol.* **2018**, *8*, 2381–2393; e) C. Martínez-Macias, M. Chen, D. A. Dixon, B. C. Gates, *Chem. Eur. J.* **2015**, *21*, 11825–11835.
- [14] a) T. V. Vernitskaya, O. N. Efimov, *Russ. Chem. Rev.* **1997**, *66*, 443–457; b) R. Ansari, *E-J. Chem.* **2006**, *4*, 186–201.

Manuscript received: October 20, 2020  
Revised manuscript received: December 7, 2020  
Accepted manuscript online: December 9, 2020